Kashf Journal of Multidisciplinary Research
Vol: 02 - Issue 1 (2025)
P-ISSN: 3007-1992 E-ISSN: 3007-200X
https://kjmr.com.pk

A NEW TOTAL VARIATION REGULARIZATION-BASED MODEL FOR ADDITIVE NOISE REMOVAL USING GLOBAL MESHLESS COLLOCATION SCHEME

Abdul Kabir

University of Engineering and Technology Mardan.

Mushtaq Ahmad Khan

University of Engineering and Technology Mardan.

Muhammad Atif

University of Engineering and Technology Mardan.

Fazal Amin

University of Engineering and Technology Mardan.

Corresponding author: Mushtaq Ahmad Khan (mushtaq@uetmardan.edu.pk)

Article Info

Abstract

In this work, we proposed a new Total Variation (TV) regularization-based model for additive noise removal problems using the Global Meshless Collocation Scheme (GMCS). This new approach not only solves the associated Partial Differential Equation (PDE) connected to the proposed model for the smooth solution regarding image restoration, and preservation of edge but also for minimization of the staircase effect due to which the image looks blocky. The experimental result demonstrates that the proposed model and meshless scheme seek to improve computational efficiency and noise removal accuracy in terms of visual efficiency and Peak-Signal-to-Noise-Ratio (PSNR) values compared to other traditional-based methods.

Keywords:

Total Variation (TV), Image Denoising, Euler-Lagrange PDE, Multi-quadratic Radial Basis Function (MQ-RBF), Additive noise, Peak-signal-to-noise-ratio (PSNR).

1. Introduction

One of the most significant features of computer vision and image processing is image denoising. The focus of this study is additive noise reduction. Image denoising aims to restore the original image by eliminating noise from a noisy image. However, because texture, edge, and noise are high-frequency components, it isn't easy to detect them during the denoising process, and the denoised images may inevitably lose some details. One of the most critical issues these days is recovering crucial information from noisy images during the noise-removal process to produce high-quality images. [1].
The additive noise model is given by

$$w_0 = w + \zeta. \quad (1)$$

Where $w: \Omega \subset \Re \to \Re^2$ represents the given true image, w_0 is the noisy image with additive noise ζ. In literature, various nonlinear approaches have been utilized to tackle this problem, such as wavelet approaches [2, 3], adaptive smoothing [4, 5], stochastic approaches [6, 7], and anisotropic diffusion [8, 9]. Recently Variational approaches have also been utilized to solve such problems, for instance, see [10, 11]. Rudin et al. (ROF) [10] provided the first TV regularization-based model for image restoration with additive noise. In this model, the TV regularization term is essential for image denoising and edge preservation. This approach produces good outcomes in the removal of image noise while maintaining the quality of edges, see [12, 13]. It also presents certain undesirable features such as the staircase effect, reduced image contrast, and increased computing time due to its nonlinearity and non-differentiability [10, 14]. The main drawback of this model is that the image restoration outcome is satisfactory in terms of quality, but it may not be visually apparent. The authors in [10] presented an artificial time-depending technique for solving the associated EL-PDE of the ROF model. The efficiency of this strategy is limited by its strict stability constraints in the time intervals. Furthermore, the time-dependent approach calculates an approximation of the solution rather than the true solution. In recent times, various methodologies have been employed to address this challenge, resulting in favorable outcomes, for instance [16–18]. But there is still room for development.

To overcome the abovementioned issue we will propose a new TV regularization-based model. We incorporate Weber's law in the regularization term of the ROF model which will examine the image visually and solve the arising non-linear associated EL-PDE of the proposed model by the Global Meshless Collocation Scheme (GMCS). This suggested approach will assist minimize the staircase effect, preserve textures, and preserve fine features throughout the restoration process in addition to aiding with image denoising and edge preservation.

In recent years, radial basis function (RBF) approaches have gained popularity in both approximation theory and the numerical solution of PDEs. The RBF collocation approach developed by Kansa [19,20], also called the Kansa method, is the most widely used RBF strategy for the latter class of problems. The meshless applications of the Kansa technique, which require only a set of points to discretize the continuous difficulty, ultimately make it so prevalent. This addition to the method's implementation is mainly simple, especially for issues involving g two or more dimensions and complex shapes. As a result, the nonlinear problem solution yields a suitable value for the shape parameter in addition to the coefficients in the RBF approximation [21]. The Kansa technique has demonstrated more effectiveness in comparison to FDM [21, 22], a pseudo-spectral method [23], and FEM [24]. For further information on RBF collocation schemes, see [21], [25, 26].

The RBF Global Meshless Collocation Scheme (GMCS) will be employed to solve the nonlinear PDE that arises in the suggested model. The primary goals of the suggested meshless scheme for image restoration are to minimize the staircase effect and preserve texture while maintaining the edges and fine details in the images through the use of the RBF interpolation process. The smoothness property and the absence of a mesh or integration procedure will yield the best restoration performance.

The remainder of the paper is organized as follows: Particular details regarding TV regularization, which is employed in the ROF model [10] for image restoration, are given in Section 2. Information about RBFs used to solve PDEs is also included in this section. Section 3 presents the suggested additive noise removal model. The related EL-PDEs for the suggested model are also included in this section. This section also includes the application of the Global Meshless Collocation Method (GMCM) for the numerical solution of the suggested model. In terms of CPU time, iterations, and the quality of the restored images, as shown by the PSNR, Section 4 gives the experimental results and a discussion of the suggested model and meshless approach in comparison to mesh-based ROF models and other meshless methods. Conclusions are included in Section 5.

2. Literature Review

2.1. TV regularization-based ROF Model for Additive Noise Removal (M1).

In their crucial work, Rudin, Osher, and Fatemi (ROF) presented an edge-preserving image de-noising model with desired mathematical features [10]. The approach, which is based on total variation, was created specifically to remove noise and other undesired fine-scale detail from images while maintaining crisp discontinuities, or edges. The most basic convex Variational model is the ROF. The minimization of this approach is as follows,

$$\widehat{w} = argmin_{w}\mathbb{E}(w) = \int_{\Omega}|\nabla w|\,dxdy + \frac{\lambda}{2}\|w - w_0\|_2^2, \tag{2}$$

where $|w| = \sqrt{w_x^2 + w_y^2}$.

The first term represents the TV regularization of $\widehat{w}$, whereas the second term represents the data fitting component. The symbol for the regularization parameter is λ. The parameter λ balances the denoising and smoothing of the denoised image, which are often affected by the amount of noise present. The EL-PDE connected with the ROF Model is as follows:

$$-\nabla\left[\frac{\nabla w}{|\nabla w|^2+\varepsilon}\right] + \lambda(w - w_0) = 0, \tag{3}$$

in $\Omega\ for\ \epsilon > 0, (x, y) \in \Re$,

or

$$-\frac{\partial}{\partial x}\left(\frac{w_x}{\sqrt{w_x^2+w_y^2}}\right) + \frac{\partial}{\partial y}\left(\frac{w_y}{\sqrt{w_x^2+w_y^2}}\right) + \lambda(w - w_0) = 0\ in\ \Omega, \tag{4}$$

with $\frac{\partial w}{\partial n} = 0$ on the boundary of $\Omega = \partial\Omega$. The time-dependent EL-PDE of equation (4) is given as follows:

$$w_t = \nabla\left[\frac{\nabla w}{|\nabla w|^2+\varepsilon}\right] + \lambda(w - w_0), \tag{5}$$

$in\ \Omega\ for\ \ t > 0, (x, y) \in \Re$,

or

$$\frac{\partial w}{\partial t} = \frac{\partial}{\partial x}\left(\frac{w_x}{\sqrt{w_x^2+w_y^2}}\right) + \frac{\partial}{\partial y}\left(\frac{w_y}{\sqrt{w_x^2+w_y^2}}\right) + \lambda(w - w_0) = 0, \tag{6}$$

in $\Omega\ for\ t > 0, (\mathfrak{x}, \mathfrak{y}) \in \Re$.

For the given $\mathcal{w}(\mathfrak{x}, \mathfrak{y}, 0)$ and also $\frac{\partial \mathcal{w}}{\partial n} = 0$ on $\partial\Omega$. For further information, see [10].

2.2. Radial Basis Function (RBF)

RBF interpolation of a continuous multivariate function, $\mathcal{f}(\mathfrak{x}), \mathfrak{x} \in \Omega \subseteq R^n$, where Ω is the bounded domain. For N interpolation function values $\{\mathfrak{y}_j\}_{i=1}^{N} \in R$ at the data location (which are traditionally called centers in the RBF concept)$\{\mathfrak{x}_j\}_{i=1}^{N} \in R^n$, then $\mathcal{f}(\mathfrak{x})$ can be approximated by a linear combination of RBFs, namely,

$$S(\mathcal{w}) = \sum_{i=1}^{N} \Gamma_i \Pi(\|\mathfrak{x} - \mathfrak{y}c_i\|), \quad (7)$$

where τ_i are unidentified coefficients that require determination. The following can be created by applying the collocation technique:

$$S(\mathfrak{x}_i) = \sum_{i=1}^{N} \Gamma_i \Pi\left(\left\|\mathfrak{x}_j - \mathfrak{y}_i\right\|\right) = \mathcal{f}(\mathfrak{x}_i), \quad (8)$$

$for\ i, j = 1,2,3,4 \ldots . N.$

$$\begin{bmatrix} \Pi(\|\mathfrak{x}_1 - \mathfrak{y}_1\|) & \Pi(\|\mathfrak{x}_1 - \mathfrak{y}_2\|) & \cdots & \Pi(\|\mathfrak{x}_1 - \mathfrak{y}_N\|) \\ \Pi(\|\mathfrak{x}_2 - \mathfrak{y}_1\|) & \Pi(\|\mathfrak{x}_2 - \mathfrak{y}_2\|) & \ldots & \Pi(\|\mathfrak{x}_2 - \mathfrak{y}_N\|) \\ \vdots & \vdots & \vdots & \vdots \\ \Pi(\|\mathfrak{x}_N - \mathfrak{y}_1\|) & \Pi(\|\mathfrak{x}_N - \mathfrak{y}_2\|) & \ldots & \Pi(\|\mathfrak{x}_N - \mathfrak{y}_N\|) \end{bmatrix} \begin{bmatrix} \Gamma_1 \\ \Gamma_2 \\ \vdots \\ \Gamma_N \end{bmatrix} = \begin{bmatrix} \mathcal{f}(\mathfrak{x}_1) \\ \mathcal{f}(\mathfrak{x}_2) \\ \vdots \\ \mathcal{f}(\mathfrak{x}_N) \end{bmatrix}. \quad (9)$$

The following matrix can represent an $N \times N$ linear system form of the aforementioned system of linear equations.

$$\mathcal{A}\Gamma = \mathcal{f}, \quad (10)$$

$$\Gamma = \mathcal{A}^{-1}\mathcal{f}, \quad (11)$$

Where $\Gamma = (\Gamma_1, \Gamma_2, \Gamma_3 \ldots . \Gamma_N)^t$, $\mathcal{f} = (\mathcal{f}_1, \mathcal{f}_2, \mathcal{f}_3, \ldots \ldots . \mathcal{f}_N)^t$ and $\mathcal{A} = \left[\Pi_{ij}\right] = \left(\mathcal{A}_{ij}\right) \epsilon\ \Re^{N \times N}$

$\mathcal{A}_{ij} = \left[\Pi_{ij}\right] = \Pi\left(\left\|\mathfrak{x}_j - \mathfrak{y}_i\right\|\right), i, j = 1,2,3, \ldots N.$ With $\Pi_{ij} = \Pi_{ji}$.

Put equation (11) in equation (8) the interpolation matric is given as:

$$\mathcal{w} = D\mathcal{f}. \quad (12)$$

For further information, see [48].

3. Proposed Model

The Rudin-Osher-Fatemi (ROF) model [10] is a TV regularization-based model for the removal of additive noise problems. The model is defined as follows:

$$\widehat{\mathcal{w}} = min_{\mathcal{w}} E(\mathcal{w}) = \mathcal{R}(\mathcal{w}) + \frac{\lambda}{2}\|\mathcal{w} - \mathcal{w}_0\|_2^2, \quad (13)$$

where

$$\mathcal{R}(\mathcal{w}) = \int_{\Omega} |\nabla \mathcal{w}|\, d\mathfrak{x}d\mathfrak{y}, \qquad \text{where } |\nabla \mathcal{w}| = \sqrt{\mathcal{w}_{\mathfrak{x}}^2 + \mathcal{w}_{\mathfrak{y}}^2}.$$

The equation (22) contains the TV regularization term denoted by $\mathcal{R}(\mathcal{w})$, and the second term represents the data fitting term. We incorporate the Weber,s law in the regularization term of the ROF model due to examine the image visually. The minimization functional of the new TV regularization-based model for additive noise removal is given below:

$$\widehat{\mathcal{w}} = min_{\mathcal{w}} \mathbb{E}(\mathcal{w}) = \ell_1 \int_{\Omega} |\nabla \mathcal{w}| d\mathfrak{x}d\mathfrak{y} + \ell_2 \int_{\Omega} \frac{|\nabla \mathcal{w}|}{\mathcal{w}} d\mathfrak{x}d\mathfrak{y} + \frac{\lambda}{2} \|\mathcal{w} - \mathcal{w}_0\|_2^2. \tag{14}$$

In order to visually evaluate the image, equation (14) uses Weber's law in the regularization term. The TV regularization component is addressed in the first part of the equation (14) and the data fitting term is indicated in the second part.

This model contains three regularization parameters indicated as ℓ_1, ℓ_2, and λ. To show an ideal balance between the restoration and the degree of smoothness displayed by the restored image, the regularization parameters are used. This new model's primary goal is to reduce noise and enhance visual efficiency by getting rid of additive noise. The resulting EL-PDE of equation (14) is given below:

$$\nabla \left(\frac{\nabla \mathcal{w}}{|\nabla \mathcal{w}|} \right) + \tilde{\lambda}(\mathcal{w}_0 - \mathcal{w}) = 0, \tag{15}$$

Where, $\tilde{\lambda} = \frac{\lambda \mathcal{w}}{(\mathcal{w}\ell_1 + \ell_2)}$.

Equation (15) can be re-written as:

$$\frac{\partial}{\partial \mathfrak{x}} \left(\frac{\mathcal{w}_{\mathfrak{x}}}{\sqrt{\mathcal{w}_{\mathfrak{x}}^2 + \mathcal{w}_{\mathfrak{y}}^2}} \right) + \frac{\partial}{\partial \mathfrak{y}} \left(\frac{\mathcal{w}_{\mathfrak{y}}}{\sqrt{\mathcal{w}_{\mathfrak{x}}^2 + \mathcal{w}_{\mathfrak{y}}^2}} \right) + \tilde{\lambda}(\mathcal{w}_0 - \mathcal{w}) = 0, \tag{16}$$

$in\ \Omega\ for\ t > 0\ (\mathfrak{x}, \mathfrak{y}) \epsilon\ \Re.$

For the given $\mathcal{w}(\mathfrak{x}, \mathfrak{y}, 0)$, and also $\frac{\partial \mathcal{w}}{\partial n} = 0$ in $\partial\Omega$.

The primary benefit of the suggested model is that it uses TV regularization and the Weberized rule to visually aspect the restored images, especially those with additive noise. Additive noise removal difficulties are addressed by this suggested model. When a proper algorithm is used, this method reduces the staircase effect and preserves the textures and edges.

3.1. Proposed Meshless Method (M2)

This subsection is concerned with the numerical solution of the EL-PDE equation (27), using the global meshless scheme (GMCM). In this approach, the functional of the Weberized law-based TV regularization-based functional is used in combination with MQ-RBF interpolation (25). The suggested mesh-free method intends to preserve sharp edges and textures in addition to efficiently restoring the image (both visually and denoising-wise) while reducing the staircase effect. Therefore, there is a consistent improvement in PSNR values and calculation time when using the proposed mesh-free technique.

Assume that $\{\mathfrak{x}\}_{i=1}^{N}$ be N_c selected center point in a closed domain $\Omega \subseteq \Re^2$ with RBF equation $\Pi(w) = \|w\|_2$ in $\Re^2$, i.e $w = (\mathfrak{x}, \mathfrak{y})$. Consequently the given known $\{\mathfrak{y}c_j\}_{j=1}^{N_c}$ N_c selected center points, the RBF interpolation is given by:

$$\mathcal{S}(\mathfrak{x}) = \sum_{i=1}^{N} \Gamma_i \Pi(\|\mathfrak{x} - \mathfrak{y}_i\|_2). \quad (17)$$

By using the following interpolation condition, the coefficient of Γ_i in equation (17) can be found.

$$\mathcal{S}(\mathfrak{x}_i) = \mathfrak{f}, \quad (18)$$

Having, a group of points converging in the middle, N_c. The RBF interpolation is illustrated using the overdetermined interpolation form in theN_c, data center.

$$\mathcal{C}\Gamma = \mathfrak{f}, \quad (19)$$

This is employed to unravel the coefficient Γ and generate, $N_c \times N_c$, a system of linear equations. Where, $\Gamma = (\Gamma_1, \Gamma_2, \Gamma_3, \dots\dots\Gamma_{N_c})^t$ and $\mathfrak{f} = (\mathfrak{f}_1, \mathfrak{f}_2, \mathfrak{f}_3, \dots\dots\mathfrak{f}_{N_c})^t$ describe $N_c \times 1$ order matrices.
In equation (19), $\mathcal{C}$ is denoted as the $N_c \times N_c$ system matrix or square interpolation and is expressed in the following manner:

$$\mathcal{C} = [\Pi_{ij}] = \left[\Pi\left(\left\|\mathfrak{x}c_i - \mathfrak{y}c_j\right\|_2\right)\right]_{1\le i,j\le N_c}. \quad (20)$$

Additionally, the matrix in equation (19) is convertible since it is positive definite which a necessary condition for a unique solution. Therefore

$$\Gamma = \mathcal{C}^{-1}\mathfrak{f}, \quad (21)$$

Furthermore, at $\{\mathfrak{x}_i\}_{i=1}^{N}$ be N evaluation data point, the RBF interpolation by using equation (17) given $N_c \times N$ matrix $\mathcal{D}$ which is written as follows:

$$\mathcal{D} = [\Pi_{ij}] = \left[\Pi\left(\left\|\mathfrak{x}_i - \mathfrak{y}c_j\right\|_2\right)\right] \quad for\ i = 1,2,3,\dots\dots N, j = 1,2,3\dots\dots\dots N_c. \quad (22)$$

There are N data points as well to approximate the over-determined condition of interpolation, the matrix-vector product is utilized to generate $\mathcal{w}$, as shown below:

$$\mathcal{w} = \mathcal{D}\Gamma. \quad (23)$$

Merging equation (21) and equation (23) results in the given equation

$$\mathcal{w} = \mathcal{D}\mathcal{C}^{-1}\mathfrak{f}, \quad (24)$$

or

$$\mathcal{w} = \mathcal{S}\mathfrak{f} \quad where\ \mathcal{S} = \mathcal{D}\mathcal{C}^{-1}. \quad (25)$$

Which represents the evaluated solution at any point in Ω. where $\mathcal{w}$ is $N \times 1$ order matrix.

Since equation (16) is

$$\frac{\partial}{\partial \mathfrak{x}}\left(\frac{w_{\mathfrak{x}}}{\sqrt{w_{\mathfrak{x}}^2+w_{\mathfrak{y}}^2}}\right)+\frac{\partial}{\partial \mathfrak{y}}\left(\frac{w_{\mathfrak{y}}}{\sqrt{w_{\mathfrak{x}}^2+w_{\mathfrak{y}}^2}}\right)+\tilde{\lambda}(w_0-w)=0, \tag{26}$$

$in\ \Omega, \frac{\partial w}{\partial \mathrm{n}}=0\ on\ the\ \Omega.$

The time marching EL-PDE of equation (26) is given as the following equation:

$$\frac{dw}{dt}=\frac{\partial}{\partial \mathfrak{x}}\left(\frac{w_{\mathfrak{x}}}{\sqrt{w_{\mathfrak{x}}^2+w_{\mathfrak{y}}^2}}\right)+\frac{\partial}{\partial \mathfrak{y}}\left(\frac{w_{\mathfrak{y}}}{\sqrt{w_{\mathfrak{x}}^2+w_{\mathfrak{y}}^2}}\right)+\tilde{\lambda}(w_0-w), \tag{27}$$

$in\ \Omega\ for\ t>0\ (\mathfrak{x},\mathfrak{y})\ \epsilon\ \Re,$

for the given $w(\mathfrak{x},\mathfrak{y},0)$ with $\frac{\partial w}{\partial n}=0$ on $\partial\Omega$. The equation (27) is re-written as

$$\frac{dw}{dt}=\frac{\left(\begin{matrix}(w_{\mathfrak{x}}^2+w_{\mathfrak{y}}^2)(w_{\mathfrak{x}\mathfrak{x}}+w_{\mathfrak{y}\mathfrak{y}})-\\(w_{\mathfrak{x}\mathfrak{x}}w_{\mathfrak{x}}+2w_{\mathfrak{x}}w_{\mathfrak{y}}(w_{\mathfrak{x}}w_{\mathfrak{y}}+w_{\mathfrak{y}}w_{\mathfrak{x}})+w_{\mathfrak{y}\mathfrak{y}}w_{\mathfrak{y}})\end{matrix}\right).}{(w_{\mathfrak{x}}^2+w_{\mathfrak{y}}^2)^{\frac{3}{2}}}+\tilde{\lambda}(w_0-w). \tag{28}$$

The implicit gradient decent scheme is applied to equation (28) we get

$$\frac{w^{(n+1)}-w^{(n)}}{dt}=\left(\frac{\begin{matrix}\left((w_{\mathfrak{x}}^2)^{(n)}+(w_{\mathfrak{y}}^2)^{(n)}\right)\left(w_{\mathfrak{x}\mathfrak{x}}^{(n)}+w_{\mathfrak{y}\mathfrak{y}}^{(n)}\right)-\\\left(2w_{\mathfrak{x}}^{(n)}w_{\mathfrak{y}}^{(n)}\left(w_{\mathfrak{x}}^{(n)}w_{\mathfrak{y}}+w_{\mathfrak{x}}w_{\mathfrak{y}}^{(n)}\right)w_{\mathfrak{x}}w_{\mathfrak{x}\mathfrak{x}}^{(n)}+w_{\mathfrak{y}}w_{\mathfrak{y}\mathfrak{y}}^{(n)}\right)\end{matrix}}{\left((w_{\mathfrak{x}}^2)^{(n)}+(w_{\mathfrak{y}}^2)^{(n)}\right)^{\frac{3}{2}}}\right)+\tilde{\lambda}\left(w_0^{(0)}-w^{(n)}\right) \tag{29}$$

Equation (29) and equation (25) together produce a nonlinear system of equations, which the GMCS is used to determine. The given equation must be taken into consideration in order to solve the nonlinear restoration system of equations.

$$G\left(w^{(n)}\right)w^{(n+1)}=G\left(w^{(n)}\right)w^{(n)}+dt\left[\left((w_{\mathfrak{x}}^2)^{(n)}+\left(w_{\mathfrak{y}}^2\right)^{(n)}\right)\left(2w_{\mathfrak{x}}^{(n)}w_{\mathfrak{y}}^{(n)}\left(w_{\mathfrak{x}}^{(n)}w_{\mathfrak{y}}+w_{\mathfrak{x}}w_{\mathfrak{y}}^{(n)}\right)+w_{\mathfrak{x}}w_{\mathfrak{x}\mathfrak{x}}^{(n)}+w_{\mathfrak{y}}w_{\mathfrak{y}\mathfrak{y}}^{(n)}\right)\right]+G\left(w^{(n)}\right)dt\left[\tilde{\lambda}\left(w_0^{(0)}-w^{(n)}\right)\right], \tag{30}$$

where $G(w)=\left(w_{\mathfrak{x}}^2+w_{\mathfrak{y}}^2\right)^{\frac{3}{2}}, w_{\mathfrak{x}}=\mathcal{S}_{\mathfrak{x}}\mathfrak{f},\ w_{\mathfrak{y}}=\mathcal{S}_{\mathfrak{y}}\mathfrak{f},\ w_{\mathfrak{x}\mathfrak{x}}=\mathcal{S}_{\mathfrak{x}\mathfrak{x}}\mathfrak{f},\ w_{\mathfrak{y}\mathfrak{y}}=\mathcal{S}_{\mathfrak{y}\mathfrak{y}}\mathfrak{f},\ \frac{\partial w}{\partial n}=w_n=\mathcal{S}_n\mathfrak{f},$ $and\ \mathfrak{f}^0=\mathfrak{f}.$

The MQ-RBF is selected for better restoration performance as a basis function in this case. The derivation has been done in a similar way as done in [27-29].

4. Result and Discussion

This section presents numerical results that illustrate the effectiveness of our suggested technique M2. The outcomes of technique M1 and the acquired results are contrasted. Figure 1 displays the test images: "Real 1 and Artificial 1."

In this study, it is expected that *N* = *Nc* = the size of the image, for our scheme M2, for the sake of comparison with scheme M1. Here, the suggested approach M2 makes use of the Multi-quadric Radial

Basis Function (MQ-RBF). The peak signal-to-noise ratio (PSNR) is taken into consideration in order to quantify the denoised image. The following formula can calculate it

$$PSNR = 10 \times log_{10}\left(\frac{M \times N max\{\hat{w}\}^2}{\|\hat{w} - w\|^2}\right). \quad (31)$$

Where $\hat{w}$ is the given image, w is the restored image and $M \times N$ is the size of an image.

Fig-1

Figure 1: Test Images

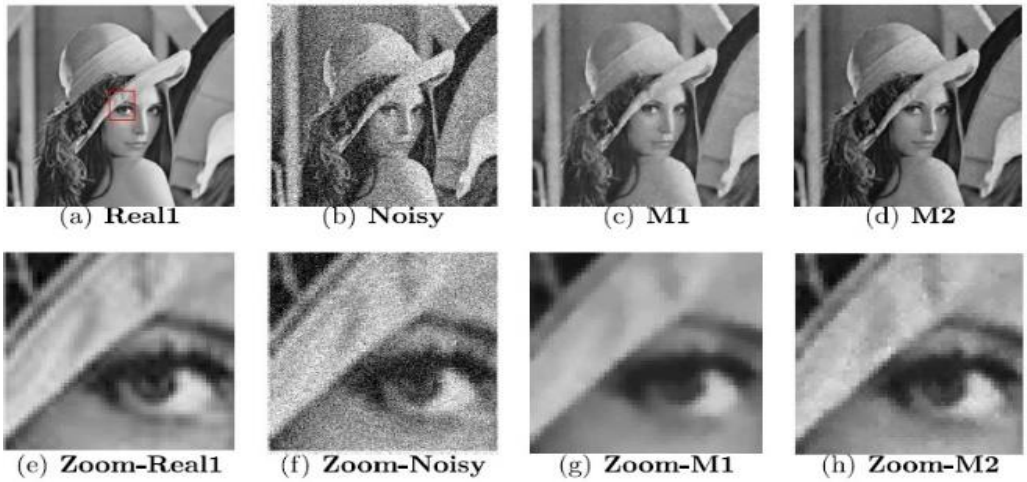

Figure 2: Left to right: (a) is true image; (b) Noisy image connected with additive Gaussian noise of $L_1 = 37\%$; (c) Restored image with M1; (d) Restored image with M2. Also zoomed-in images for staircase effect of true, noisy, restored by M1 and M2 are given in (e), (f), (g), and (h).

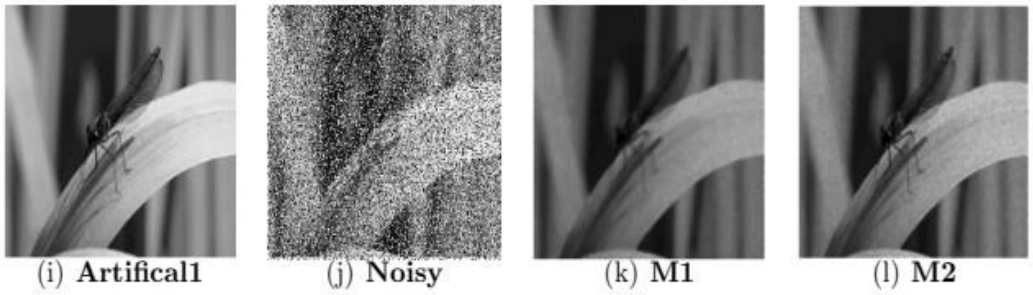

Figure 3: Left to right; (f) True image; (g) Noisy image connected with salt and pepper noise of $L_2 = 40\%$; (h) Obtained by M1; (i) Obtained by M2.

Table: 1 PSNR values, number of iterations required for convergence, and CUP time comparison of Algorithm M1 and M3.

Image	Size	M1			M3		
		PSNR	Iters	Time(s)	PSNR	Iters	Time(s)
Real1	256^2	28.22	29	13.59	28.67	18	9.38
Artifical1	256^2	23.93	34	16.70	24.30	27	10.79

Test Problem:

In this investigation, Real1 and Artifical1 images have been taken for image restoration having additive Gaussian and salt and pepper noise with noise levels $L_1 = 37\%$ and $L_2 = 40\%$, respectively. The true images are given in Figures 2 and 3 as (a), (e) and (i) respectively while the noisy images are represented by (b), (f), and (j), respectively. The mesh-based method M1 used on the ROF model produces a good restoration result but produces the staircase effect which is the main drawback of the M1 and ROF model. Also, the restoration results are also affected a bit due to the nonlinearity and non-differentiability of the associated EL-PDE. All these images are shown in Figures 2 and 3 as (c), (g) and (k), respectively. But the restoration results i.e., image denoising, preservation of edges and reduction of staircase effects obtained by the proposed model and meshless scheme M2 are far better than M1 due to the application of the new model and meshless method with applications of adaptive nature, and MQ-RBF applied on them [20]. Similarity, due to the additional application of Weberized law involved in the proposed model makes results effective in visual representation compared to the model M1 applied on the ROF model. These obtained images are shown in Figures 2 and 3 as (d), (h) and (l), respectively. It can also be noticed from Table 1 that the PSNR values of M2 are greater than M1 which shows the best restoration performances of M2 over M1. Also, Table 1 indicates that the number of iterations and time required for convergence of M2 are less than M1 which shows the quick restoration performance of M2 due to its meshless applications and easy implementation in comparison to M1.

5. Conclusion

In this paper, a novel TV-based approach for removing additive noise from noisy image data is presented. The GMCS solves the associated EL-PDE with a new model for a smooth solution that uses the MQ-RBF as the basis function. This solution is adaptable and computationally easy because of the meshless and MQ-RBF features. In comparison to the ROF Model, the outcomes are determined based on visual quality and PSNR value, staircase effect minimization, and texture and edge preservation. The new model and corresponding meshless technique are tested on both artificial and actual images, and the outcomes are contrasted with those of conventional techniques and ROF models. The experimental results showed that the suggested model and meshless approach are significantly better at image restoration PSNR values (image denoising and visual efficiency due to the proposed model) and other related aspects, such as the preservation of blocky effects, texture, and sharp edges, the number of iterations needed for convergence, and the CPU time (proposed method).

References

1. R. C. Gonzalez and R. E. Woods, *Digital Image Processing*, 3rd ed. Englewood Cliffs, NJ, USA: Prentice-Hall, 2008.
2. Li, X., Li, L., & Wang, Q. H. (2018). Wavelet based iterative perfect reconstruction in computational integral imaging. *JOSA A*, *35*(7), 1212-1220.
3. Naveed, K., Shaukat, B., Ehsan, S., Mcdonald Maier, K. D., & Ur Rehman, N. (2019). Multiscale image denoising usinggoodness-of-fit test based on EDF statistics. *PLoS One*, *14*(5), e0216197.
4. Kervrann, C. (2004). An adaptive window approach for image smoothing and structures preserving. In *Computer Vision-ECCV 2004: 8th European Conference on Computer Vision, Prague, Czech Republic, May 11-14, 2004. Proceedings, Part III 8* (pp. 132-144). Springer Berlin Heidelberg.
5. Polzehl, J., & Tabelow, K. (2007). Adaptive smoothing of digital images: The R package adimpro.
6. Ramadhan, A., Mahmood, F., & Elci, A. (2017). Image denoising by median filter in wavelet domain. *arXiv preprint arXiv:1703.06499*.
7. Luo, L., Zhao, Z. Q., Li, X. P., & Feng, X. C. (2019). A stochastic image denoising method based on adaptive patch size. *Multidimensional Systems and Signal Processing*, *30*, 705-725.
8. Bai, J., & Feng, X. C. (2018). Image denoising using generalized anisotropic diffusion. *Journal of Mathematical Imaging and Vision*, *60*, 994-1007.
9. Liu, F., & Liu, J. (2012). Anisotropic diffusion for image denoising based on diffusion tensors. *Journal of Visual Communication and Image Representation*, *23*(3), 516-521.
10. Rudin, L. I., Osher, S., & Fatemi, E. (1992). Nonlinear total variation based noise removal algorithms. *Physica D: nonlinear phenomena*, *60*(1-4), 259-268.
11. Russ, J. C., & Russ, J. C.(2017). *Introduction to image processing and analysis*. CRC press.
12. Osher, S., Burger, M., Goldfarb, D., Xu, J., & Yin, W. (2005). An iterative regularization method for total variation based image restoration. *Multiscale Modeling & Simulation*, *4*(2), 460-489.
13. Chan, T., Esedoglu, S., Park, F., & Yip, A. (2006). Total variation image restoration: Overview and recent developments. *Handbook of mathematical models in computer vision*, 17-31.
14. Chang, Q., Tai, X. C., & Xing, L. (2009). A compound algorithm of denoising using second-order and fourth-order partial differential equations. *Numer. Math. Theory Methods Appl*, *2*, 353-376.
15. Thanh, D. N., Prasath, V. S., Hieu, L. M., & Dvoenko, S. (2020). An adaptive method for image restoration based on high-order total variation and inverse gradient. *Signal, Image and Video Processing*, *14*(6), 1189-1197.
16. Jiang, D. H., Tan, X., Liang, Y. Q., & Fang, S. (2015). A new nonlocal variational bi regularized image restoration model via split Bregman method. *EURASIP Journal on Image and Video Processing*, *2015*, 1-10.
17. Xu, H., Sun, Q., Luo, N., Cao, G., & Xia, D. (2013). Iterative nonlocal total variation regularization method for image restoration. *PloS one*, *8*(6), e65865.
18. Guo, J., & Chen, Q. (2021). Image denoising based on nonconvex anisotropic total variation regularization. *Signal Processing*, *186*, 108124.
19. Kansa, E. J. (1990). Multiquadrics—A scattered data approximation scheme with applications to computational fluid dynamics—I surface approximations and partial derivative estimates. *Computers & Mathematics with applications*, *19*(8 9), 127-145.
20. Kansa, E. J. (1999). Motivation for using radial basis functions to solve PDEs. *RN*, *64*(1), 1.
21. Jankowska, M. A., Karageorghis, A., & Chen, C. S. (2018). Kansa RBF method for nonlinear problems. *Boundary Elements and Other Mesh Reduction Methods*, *39*.

22. Zerroukat, M., Power, H., & Chen, C. (1998). A numerical method for heat transfer problems using collocation and radial basis functions. *International Journal for numerical methods in Engineering*, *42*(7), 1263-1278.
23. Larsson, E., & Fornberg, B. (2003). A numerical study of some radial basis function based solution methods for elliptic PDEs. *Computers & Mathematics with Applications*, *46*(5-6), 891-902.
24. Li, J., Cheng, A. H. D., & Chen, C. S. (2003). A comparison of efficiency and error convergence of multiquadric collocation method and finite element method. *Engineering Analysis with Boundary Elements*, *27*(3), 251-257.
25. Parand, K., & Rad, J. A. (2012). Numerical solution of nonlinear Volterra Fredholm-Hammerstein integral equations via collocation method based on radial basis functions. *Applied Mathematics and Computation*, *218*(9), 5292-5309.
26. Doha, E. H., Baleanu, D., Bhrawy, A. H., & Abdelkawy, M. A. (2013). A Jacobi Collocation Method for Solving Nonlinear Burgers-Type Equations. In *Abstract and Applied Analysis* (Vol. 2013, No. 1, p. 760542). Hindawi Publishing Corporation.
27. Khan, M. A., Chen, W., Ullah, A., & Fu, Z. (2017). A mesh-free algorithm for ROF model. *EURASIP Journal on Advances in Signal Processing*, *2017*, 1-16.
28. Ahmad Khan, M., Altamimi, A., Hussain Khan, Z., Shehzad Khattak, K., Khan, S., Ullah, A., & Ali, M. (2021). Multiquadric radial basis function approximation scheme for solution of total variation based multiplicative noise removal model. *Computer Modeling in Engineering & Sciences*, *126*(1), 55-88.
29. Khan, M. A., Altamimi, A. B., Khan, Z. H., Khattak, K. S., Ali, M., Ullah, A., ... & Abrar, M. F. (2020). Total Variation Filter via Multiquadric Radial Basis Function Approximation Scheme for Additive Noise Removal. *IEEE Access*, *8*, 88241-88258.